# STRUCTURAL AND MAGNETIC PROPERTIES OF Mg-Co FERRITE NANOPARTICLES

A. M. MOHAMMAD[a,*] , S. M. ALI RIDHA[b], T. H. MUBARAK[c]
[a]*University of Garmian, College of Education, Department of Physics*
[b]*University of Kirkuk, College of Education for Pure Science, Department of Physics*
[c]*University of Diyala, College of Science, Department of Physics*

A series of magnesium-substituted cobalt ferrite nanoparticles $Co_{1-x}Mg_xFe_2O_4$ ($0.0 \leq x \leq 1.0$, step 0.2), have been synthesized using sol–gel auto-combustion method. The powders calcined at 600, 700, and 800 ˚C for 3h. Various characterization methods were used to investigate the prepared powders such as X-ray diffraction (XRD), field emission scanning electron microscopy (FE-SEM), and vibrating sample magnetometer (VSM). The XRD patterns of the synthesized samples confirm the formation of single phase spinal structured nanoparticles. FE-SEM image results show some agglomerated of spherical and polyhedral shape morphology. Moreover, the average crystallite size was found to be ranging from (55.146-68.434nm). Saturation magnetization ($M_s$), remanent magnetization ($M_r$), and coercivity ($H_c$) decreases with increase in Mg substitution as indicated by VSM at room temperature. Both the structural and magnetic properties of Mg-Co ferrite nanoparticles depend upon $Mg^{2+}$ ions substitution.

(Received March 23, 2018; Accepted July 5, 2018)

*Keywords:* Nanoparticles, Spinal ferrites, Sol-gel auto-combustion, X-ray diffraction, FR-SEM, VSM

## 1. Introduction

The synthesis of ferrite nanoparticles and its modification has been studied in recent years to enhance structural, electrical, and magnetic properties of nanomaterials, to make a potential material for wide range of applications such as high-density data storage, micro-wave devices, magnetic fluids, high frequency magnets, and magnetic refrigeration [1, 2]. The presence of some substituting divalent or trivalent elements in ferrite nanoparticles during the synthesis and processing, alter the distribution of the metal ions and hence their properties [3] The general molecular formula of materials having spinel structure is $AB_2O_4$ in which $A^{2+}$ and $B^{3+}$ are the divalent and trivalent ions respectively [4]. The most familiar kind of magnetic spinel materials is cobalt ferrite ($CoFe_2O_4$), due to its excellent properties, such as its relatively high saturation magnetization ($M_s$), coercivity ($H_c$) and magnetic anisotropy [5, 6]. Cobalt ferrite is a well-known hard magnetic material, with complete inverse spinel or partial inverse spinel structures depending on cation substitution or heat treatment [7, 8]. The $Co^{2+}$ ions have preference for the octahedral site, while $Fe^{3+}$ ions distribute equally between tetrahedral and octahedral sites [9]. The structural, electrical and magnetic properties of ferrites are highly sensitive to conditions of their synthesis methods, compositions, magnetic interactions and distribution of cations at tetrahedral and octahedral sites [5]. Any change in distribution of cations among tetrahedral site and octahedral site by cations substitution have very dominant effects on the physical properties, the substitutions of magnetic or non-magnetic ions alters the spin order which affects the magnetic and electric properties of ferrite structure and greatly affect the ferrite overall properties [10, 11]. The substitution of non-magnetic magnesium $Mg^{2+}$ ion can modify the properties of cobalt ferrite [12]. The cation distribution according to the earlier reported reveals that $Mg^{2+}$ ions exist in both sites (A and B) but have a strong preference for the octahedral (B) site [13]. Various methods such as

*Corresponding author: ali.mustafa@garmian.edu.krd

ceramic [14], co-precipitation [15], sol–gel [16], hydrothermal [17], microemulsion [18], and combustion methods [19] are used for the preparation of spinel ferrites. The present work reports the compositional dependence of the structural and magnetic properties of $Mg^{2+}$ substituted $CoFe_2O_4$ nanoparticles having the general chemical formula $Co_{1-x}Mg_xFe_2O_4$ ($0.0 \leq x \leq 1.0$, step 0.2) synthesized by sol-gel auto-combustion method. The $Mg^{2+}$ ions substitution causes appreciable changes in the structural and magnetic properties of the nanoferrites, the influence of $Mg^{2+}$ ions substitution in $CoFe_2O_4$ ferrite has been investigated by XRD, FE-SEM, and VSM at room temperature.

## 2. Experimental details

### 2.1. Materials and methods

Nanoparticles of magnesium substituted cobalt ferrites $Co_{1-x}Mg_xFe_2O_4$ (x=0.0, 0.2, 0.4, 0.6, 0.8, 1.0) were synthesized in air using sol-gel auto-combustion method. Stoichiometric amounts of ferric nitrate $Fe(NO_3)_3.9H_2O$, cobalt nitrate $Co(NO_3)_2.6H_2O$, magnesium nitrate $Mg(NO_3)_2.6H_2O$ and citric acid $C_6H_8O_7$ in mole ratio of 1:1 were weighed and dissolved separately in minimum amount of deionized water to form a mixed solution. After stirring the solutions were mixed and pH of the resulting solution was adjusted to 7 by adding ammonia solution drop wise [20]. The obtained solutions were transformed into a viscous gel phase by slowly increasing the temperature of hot plate to 90 °C for 2 h under continuous stirring. When the gel was formed, the temperature of the gel increased and at a certain temperature approximately 200 °C a large amount of gases liberated and the auto-combustion of gel took place and the gel was converted to as-burnt ferrite powder. The final as-burnt powders were then thermally calcined at 600, 700, and 800 ˚C for 3h to remove organic waste and to improve the homogeneity of the samples, then it used for further investigations of structural and magnetic properties.

### 2.2. Characterizations

The crystal structure of the synthesized samples were characterized using X-Ray Diffraction (XRD), model PANalytical (X'pert Pro, Netherlands) equipped with high-intensity Cu kα radiation source (λ= 0.154 nm, 40 mA, 40 kV) in the 2θ range (15° - 80°). Morphology of the calcined powders at 700 ˚C was observed by Field Emission Scanning Electron Microscopy (FE-SEM), using (FE-SEM; Model Mira3-XMU, TESCAN, japan). The magnetic properties of the calcined powders at 700 ˚C have been investigated by means of Vibrating Sample Magnetometer (VSM), using a (LBKFB model Meghnatis Daghigh Kavir Company) in applied field ranging from −15 to + 15 kOe at room temperature.

## 3. Results and discussion

### 3.1. Structural properties

The XRD patterns of Mg-substituted cobalt ferrite $Co_{1-x}Mg_xFe_2O_4$ (x=0.0, 0.2, 0.4, 0.6, 0.8, and 1.0) for as-burnt and the calcined powders at different temperature 600, 700 and 800℃ are shown in Fig. 1(a-f). The XRD pattern shows that all the reflection peaks corresponding to (220), (311), (222), (400), (422), (511) and (440) planes in pure (x=0) and different Mg substituted cobalt ferrites. The peak position in XRD patterns are perfectly matched the standard pattern with reference code ICSD 00-001-1121 for pure $CoFe_2O_4$ and 98-011-2788 with 98-011-0946 for Mg substituted $CoFe_2O_4$ and $MgFe_2O_4$, respectively. All the major peaks corresponding to the pure single spinel *fcc* phase remained unchanged as a result of substitution, while a peak designated by symbol * may be due to the presence of hematite (iron oxide). Our results show that, as the calcination temperature increases, the diffraction peaks become sharper and narrower, and their intensity increases. This indicates intensification in crystallinity that originates from the growing of crystalline volume ratio due to the particle size enlargement of the nuclei [21] which is well agreed with the earlier report [22].

The crystallite sizes ($D$) for each sample was estimated from Scherrers formula [23, 24] using the peak width at half maximum intensity (FWHM) peak (311).

$$D = \frac{0.96\lambda}{\beta.\cos\theta} \tag{1}$$

where $D$ is the crystalline size, $\lambda$ the wavelength of X-ray, and $\beta$ is the full width at half maximum of the concerned peak.

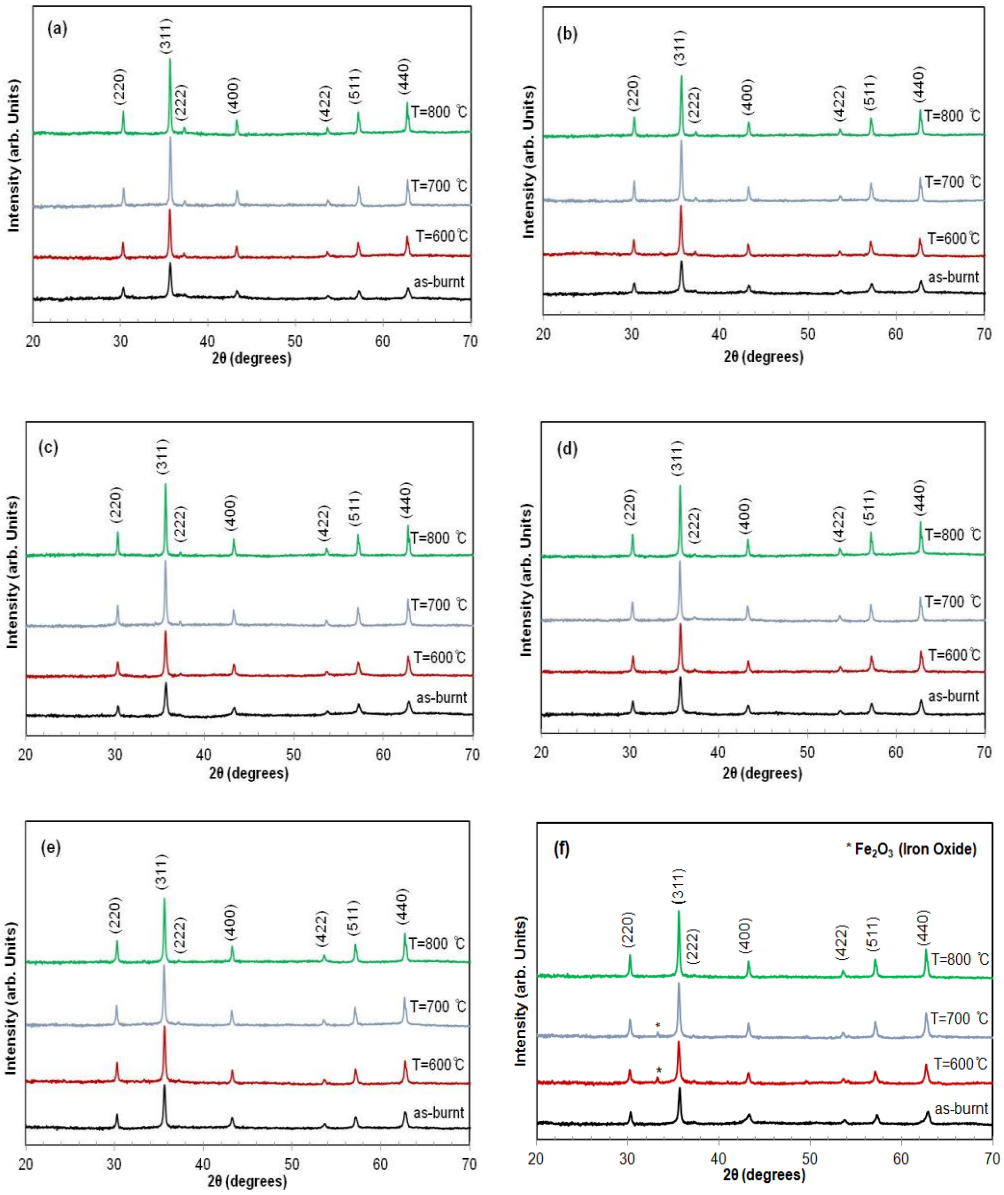


*Fig. 1. XRD patterns of $Co_{1-x}Mg_xFe_2O_4$ nanoparticles (a) x =0.0, (b) x =0.2, (c) x =0.4, (d) x =0.6, (e) x =0.8 and (f) x =1.0.*

The value of crystallite size ($D$) for the un-substituted cobalt ferrite sample (x=0.0) for as-burnt is 38.791 nm which is comparable with crystallite size 33.686 nm observed for cobalt ferrite by Muthurani et al [25]. The Mg substituted cobalt ferrite with (x = 0.2-1.0) shows a lower grain growth and the crystallite size ($D$) lies in the range of 33.495 - 37.913 nm. The varying of

crystalline size in Table 1, is understandable in terms of different nature of driving force for grain boundaries motion and retarding force by pores in these particular ferrites [5].

Table 1, clearly shows as the calcining temperature increases the crystalline size increase. Herein, the specific surface area of the particle decreases as the calcined temperature increase, this is observed in an earlier report[26].

The lattice constant (*a*) of $Co_{1-x}Mg_xFe_2O_4$ spinel ferrite nanoparticles has been calculated by d-spacing using the following relation [12].

$$a = d_{hkl}\sqrt{h^2 + k^2 + l^2} \tag{2}$$

where *h*, *k* and *l* are the Miller indices of the lattice plane and $d_{hkl}$ is interplanar spacing. As shown in Table 1, with reference to the un-substituted cobalt ferrite sample the lattice parameters for as-burnt at (x=0) initially decreased from 8.361 Å to 8.355 Å at (x=0.4), some increase appear in value of lattice parameters 8.359 Å at (x=0.6) and later decreased to 8.353 Å at (x=1.0) with increase *x*. The resultant variation in lattice parameter does not appear to be a simple linear function. Based on the fact that the radius of $Mg^{2+}$ ions (0.72 Å) has a smaller ionic radius compared to that of $Co^{2+}$ ions (0.745Å). The lattice parameter was expected to decrease as the substituted magnesium content increases assuming that it follows Vegard's law [27], a simple possible interpretation for the observed occurrence might possibly be due to the change in $Mg^{2+}$ substitue rate in the tetrahedral and octahedral sites with increase in $Mg^{2+}$ concentration.

The X-ray density ($\rho_x$) is dependent on the molar mass of the synthesized compounds and the lattice parameter (*a*) which was calculated using the relation [28].

$$\rho_x = \frac{8M}{Na^3} \tag{3}$$

where 8 is the number of molecules per unit cell, *N* is Avogadro's number and *M* is the molecular weight. For as burnt samples the value of ($\rho_x$) decreases linearly, it directly correlates with the decrease of molecular weight; however, it decreased with $Mg^{2+}$ substitutions for all prepared samples and was in the range 5.332 to 4.558 g/cm$^3$. This was attributed to the fact that atomic weight of the magnesium is less than that of cobalt.

The distance between the magnetic ions, known as hopping length *L*, influences the physical properties of the ferrite system; the hopping length in A-site $L_A$ (tetrahedral) and B-site $L_B$ (octahedral) were calculated using the relations below [29].

$$L_A = 0.25a\sqrt{3} \tag{4}$$

$$L_B = 0.25a\sqrt{2} \tag{5}$$

The calculated values of the hopping length $L_A$ and $L_B$ of different compositions were tabulated in Table 1. It is observed that the hopping length changes as the Mg-substitution and calcination temperature changes. The rate changes, at which $Mg^{2+}$ substitutes into the tetrahedral and octahedral sites with increase in $Mg^{2+}$ concentration, may be playing a vital role in altering the value of hopping length which is related to the fact that $Mg^{2+}$ ion has smaller radius than $Co^{2+}$ion.

*Table 1. Values of crystallite size (D), Lattice parameter (a), X-ray density ($\rho_x$), hopping length ($L_A$) and ($L_B$) of $Co_{1-x}Mg_xFe_2O_4$ nanoparticle.*

| ***X*** | ***Composition*** | ***Temp. ˚C*** | ***D(nm)*** | ***a(Å)*** | ***$\rho_x$ (gm/cm$^3$)*** | ***$L_A$(Å)*** | ***$L_B$(Å)*** |
|---|---|---|---|---|---|---|---|
| **0** | (CoFe2O4) | as- burnt | 38.791 | 8.361 | 5.332 | 3.6204 | 2.9561 |
| | | 600 | 49.638 | 8.370 | 5.315 | 3.6241 | 2.9591 |
| | | 700 | 54.161 | 8.354 | 5.345 | 3.6174 | 2.9536 |
| | | 800 | 59.149 | 8.362 | 5.329 | 3.6210 | 2.9565 |
| **0.2** | ($Co_{0.8}Mg_{0.2}Fe_2O_4$) | as-burnt | 33.495 | 8.360 | 5.176 | 3.6201 | 2.9558 |
| | | 600 | 48.202 | 8.372 | 5.154 | 3.6252 | 2.9600 |
| | | 700 | 54.156 | 8.362 | 5.172 | 3.6209 | 2.9564 |
| | | 800 | 52.454 | 8.360 | 5.176 | 3.6200 | 2.9557 |
| **0.4** | ($Co_{0.6}Mg_{0.4}Fe_2O_4$) | as-burnt | 34.753 | 8.355 | 5.028 | 3.6177 | 2.9538 |
| | | 600 | 44.127 | 8.361 | 5.016 | 3.6206 | 2.9562 |
| | | 700 | 53.460 | 8.364 | 5.011 | 3.6217 | 2.9571 |
| | | 800 | 59.150 | 8.361 | 5.017 | 3.6203 | 2.9560 |
| **0.6** | ($Co_{0.4}Mg_{0.6}Fe_2O_4$) | as-burnt | 37.910 | 8.359 | 4.864 | 3.6194 | 2.9552 |
| | | 600 | 47.389 | 8.358 | 4.865 | 3.6190 | 2.9549 |
| | | 700 | 55.593 | 8.372 | 4.840 | 3.6252 | 2.9600 |
| | | 800 | 57.515 | 8.365 | 4.852 | 3.6223 | 2.9576 |
| **0.8** | ($Co_{0.2}Mg_{0.8}Fe_2O_4$) | as-burnt | 37.739 | 8.358 | 4.707 | 3.6191 | 2.9550 |
| | | 600 | 48.209 | 8.360 | 4.704 | 3.6200 | 2.9557 |
| | | 700 | 51.795 | 8.372 | 4.684 | 3.6251 | 2.9599 |
| | | 800 | 55.232 | 8.362 | 4.701 | 3.6208 | 2.9564 |
| **1.0** | ($MgFe_2O_4$) | as-burnt | 37.913 | 8.353 | 4.558 | 3.6168 | 2.9531 |
| | | 600 | 36.897 | 8.373 | 4.525 | 3.6257 | 2.9604 |
| | | 700 | 46.073 | 8.370 | 4.531 | 3.6242 | 2.9591 |
| | | 800 | 53.115 | 8.371 | 4.529 | 3.6246 | 2.9595 |

### 3.2. FE-SEM studies

The surface morphology and particle size of Mg-Co ferrite nanoparticles $Co_{1-x}Mg_xFe_2O_4$ ($x$ = 0.0, 0.4, and 1.0) calcined at 700 ˚C have been investigated by FE-SEM image as shown in Fig. 2 (a–c).

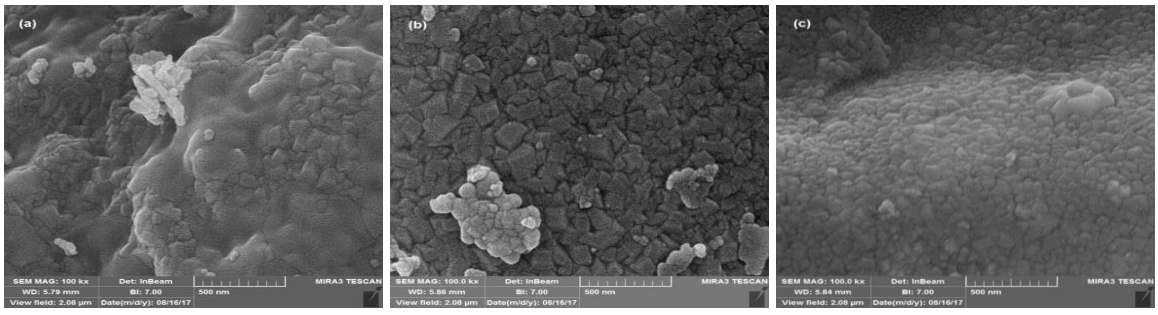


*Fig. 2. FE-SEM micrographs of $Co_{1-x}Mg_xFe_2O_4$ nanoparticles calcined at 700 ˚C, (a) x=0. (b) x=0.4 and (c) x=1.*

From the images, one can notice the micrographs of Mg-Co ferrite nanoparticles reveal that the microstructure of the ferrites were affected by the substitution of Mg-ions and shows

porous structure, with high agglomerated and homogenous spherical and polyhedral particles. In Fig. 2 (a and b) images, the particles have polyhedral shape with fine size, while the Fig. 2 (c) shows a homogeneous microstructure and spherical shape with narrow particle size distribution. The formation of the porous structure of the ferrite samples may be due to the release of excess amount of gases during combustion method [30]. The appearance of some agglomerated areas in the FE-SEM images was due to the natural occurring interaction between magnetic nanoparticles and the thermal process. In many cases of nanocrystalline spinel ferrites, there is a tendency of nanoparticles to agglomerate [31].

*Table 2. Average particle sizes of $Co_{1-x}Mg_xFe_2O_4$ nanoparticles calcined at 700 ˚C with (x = 0.0, 0.4, and 1.0) determined from XRD and FE-SEM.*

| ***Mg content*** | ***Concentration*** | ***D(nm) XRD*** | ***D(nm) FE-SEM*** |
|---|---|---|---|
| 0.0 | ($CoFe_2O_4$) | 54.182 | 68.434 |
| 0.4 | ($Co_{0.6}Mg_{0.4}Fe_2O_4$) | 53.481 | 65.082 |
| 1.0 | ($MgFe_2O_4$) | 46.091 | 55.146 |

Table 2 demonstrates that the values of the estimated diameters of the $Co_{1-x}Mg_xFe_2O_4$ nanoparticles with (x = 0.0, 0.4, and 1.0) calcined at 700 ˚C with relatively well crystallized grains and an average particle size smaller than 68.434, 65.082, and 55.146 nm respectively, measured by Image J Software (version 1.51j8; National Institutes of Health, Bethesda, USA).

It is observed that the difference in the particle size for the present samples calculated by FE-SEM and the crystallite size obtained using Scherrer's formula from XRD, may be because of the molecular structural disorder and lattice strain, which results from the different ionic radii and/or clustering of the nanoparticles. Hence, the XRD method has a more stringent criterion and leads to smaller sizes [1, 32].

### 3.3. Magnetic measurement

The magnetic properties of synthesized $Co_{1-x}Mg_xFe_2O_4$ nanoparticles with x=0.0, 0.2, 0.5, 0.8 and 1.0 calcined at 700℃ have been determined at room temperature by means of Vibrating Sample Magnetometer (VSM) in the applied field ranging from −15 to +15 kOe as shown in Fig. 3.

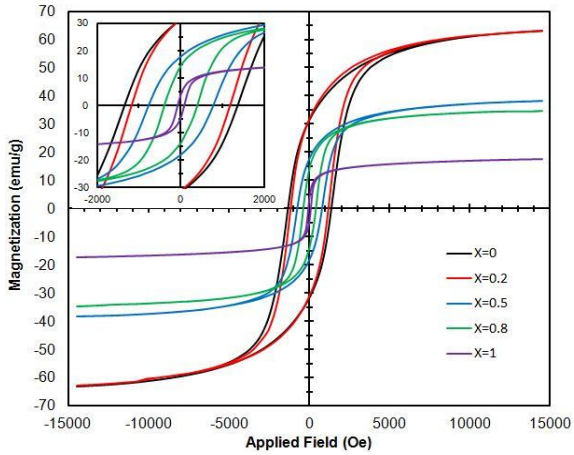


*Fig. 3. Hysteresis loops of Mg-substituted cobalt ferrite $Co_{1-x}Mg_xFe_2O_4$ nanoparticles with (x= 0.0, 0.2, 0.5, 0.8 and 1.0) calcined at 700 ˚C.*

The saturation magnetization ($M_s$) of Mg–Co ferrite materials was evaluated from Hysteresis loop, and the magnetic moment ($n_B$) in ($\mu_B$) per unit formula was computed using following relation [33].

$$n_B = \frac{M_{wt} \times M_s}{5585} \tag{6}$$

where, $M_{wt}$ is the molecular weight. The values of saturation magnetization and magnetic moments are presented in Table 3. The saturation magnetization and magnetic moment decreases with increasing Mg substitution, being 63.18 emu.g$^{-1}$ (=2.65 $\mu_B$) and 17.47 emu.g$^{-1}$ (=0.63 $\mu_B$), for x=0.0 and x=1.0 respectively. This decrease in $M_s$ with increasing Mg substitution may be attributed to the cation distribution among A and B-sites in the spinel structure because $Mg^{2+}$ ion is nonmagnetic, which are well agreed with the earlier reports [34].

The increasing of Mg-substitution, lead to decrease of saturation magnetization ($M_s$) due to fact that substitution $Mg^{2+}$ prefers to occupy octahedral site and probably transfers $Fe^{3+}$ ions to the A site which in turn, leads to decrease in net magnetization. The concentration and type of cations also have dominant effect on magnetic properties [35]. The values of magnetic moment ($n_B$) which goes on decreasing with increasing Mg content in cobalt ferrite should result in continuous decrease in magnetization as observed in this study. It is noteworthy that a similar trend was observed when Al was substituted for $Fe^{3+}$ [36].

The remanent magnetization ($M_r$) is the magnetization left behind in a ferromagnetic material after an external magnetic field is removed. The values of remanent magnetization are evaluated from the hysteresis loop, and its value for un-substituted cobalt ferrite (x=0) and Mg-substituted cobalt ferrite (x=1.0) are 31.77 and 4.12 emu.g$^{-1}$ respectively. Table 3 shows the compositional variation and the ratio of remanent magnetization ($M_r$) over saturation magnetization ($M_s$) at room temperature. In other words, this ratio ($M_r/M_s$) is called squareness, it is an important characteristic parameter for applications of ferromagnetic materials. For $Co_{1-x}Mg_xFe_2O_4$ nanoparticles (x = 0.0, 0.2, 0.4, 0.6, 0.8 and 1.0), this parameter reduces, mostly because of the fact that the amount of Co content lessens. Similar trend was observed for Mn substituted cobalt ferrite [37]. In the present study the squareness ratio ($M_r/M_s$) for un-substituted cobalt ferrite is found 0.50 at room temperature, which is leaser comparable to that observed by Aghav et al (0.92) [38], and higher than that reported by Atiq et al (0.43) [5]. When the squareness ratio is less than 0.5 the particles interact by magnetostatic interactions and the exchange coupled interaction survives when squareness ratio is higher than 0.5 [39]. In this study, all properties possess squareness ratio values less than 0.5 indicating that the particles interact by magnetostatic interactions

The coercive field or coercivity ($H_c$) is the magnitude of the field that must be applied in the negative direction to bring the magnetization of the sample back to zero. The coercivity values of prepared Mg-substituted cobalt ferrites were recorded from the hysteresis loop and listed in table 3. The coercivity of the ferrite decreases with increase in Mg concentration. As suggested by Atiq et al [5]. The coercive force ($H_c$) in the present study is 1350 $O_e$ for un-substituted cobalt ferrite, which is less than the coercivity value of 2478 Oe as observed by Aghav et al [38], and higher than that reported by Atiq et al 680.20 $O_e$ [5].

Moreover, the dependence of magnetic anisotropy ($K$) for different Mg-substituted cobalt ferrites was evaluated using following relation [40].

$$H_c = \frac{0.96 \times K}{M_s} \tag{7}$$

From Table 3 it is observed that magnetic anisotropy $K$ decreases with increasing $Mg^{2+}$ content. This result can be thought in terms of the effects of Mg-substitution on the site occupancies of the cations, the strong magnetic anisotropy of cobalt ferrite is primarily due to the presence of $Co^{2+}$ ions on the octahedral (B) sites. Therefore if $Mg^{2+}$goes into the octahedral sites and at least some of the $Co^{2+}$ ions are displaced from octahedral site to tetrahedral sites, then $K$

decreases [34]. Magnesium ferrite has lower magnetic anisotropy than cobalt ferrite. Therefore Mg-substitution to the cobalt ferrite reduces the magnetic anisotropy of the sample. From these observations it may be concluded that as the Mg composition (x) is increasing from (0 to 1) in the cobalt ferrite, the coercivity is found to decrease gradually. This means that the ferrite material becomes softer as regards to its magnetic properties [5, 40], and the gradual decrease in coercivity depicts that hard magnetic cobalt ferrite becomes the soft magnetic material on substitution of Mg at Co site.

*Table 3. Variation in saturation magnetization ($M_s$), remanance magnetization ($M_r$), coercivity ($H_c$), magnetic moment ($n_B$), squareness ratio ($M_r/M_s$), and magnetic anisotropy (K) of Mg- subsitiuted cobalt ferrite $Co_{1-x}Mg_xFe_2O_4$ with (x= 0.0, 0.2, 0.5, 0.8 and 1.0) calcined at 700 ˚C.*

| ***Mg content (x)*** | $M_s$ ***(emu $g^{-1}$)*** | $M_r$ ***(emu $g^{-1}$)*** | $H_c$ ***($O_e$)*** | $n_B$ ***($\mu_B$)*** | $M_r/M_s$ | $K \times 10^3$ ***(emu .$O_e$ $g^{-1}$)*** |
|---|---|---|---|---|---|---|
| 0.0 | 63.18 | 31.77 | 1350.35 | 2.65 | 0.50 | 88.87 |
| 0.2 | 63.02 | 31.25 | 1181.27 | 2.57 | 0.50 | 77.55 |
| 0.5 | 38.24 | 17.93 | 772.84 | 1.49 | 0.47 | 30.79 |
| 0.8 | 34.66 | 14.55 | 395.30 | 1.28 | 0.42 | 14.27 |
| 1.0 | 17.47 | 4.12 | 78.78 | 0.63 | 0.24 | 1.43 |

## 4. Conclusions

Magnesium substituted cobalt ferrite nanoparticles $Co_{1-x}Mg_xFe_2O_4$ (x= 0, 0.2, 0.4, 0.6, 0.8 and 1.0) have been synthesized using a sol–gel auto-combustion method, the powders calcined at 600 , 700, and 800 ˚C for 3h. The effect of Mg-substituted on structural and magnetic properties of $CoFe_2O_4$ has been studied. The X-ray diffraction analysis has confirmed the formation of single phase spinel structure. FE-SEM image results show the some agglomerated of spherical and polyhedral shape morphology with fine size. Magnetization measurement shows that an increase in $Mg^{2+}$ substitution reduces the saturation magnetization, remanent magnetization, coercivity and magnetic moment. Moreover, substitution of magnesium into the cobalt ferrite alters its magnetic properties and transforms cobalt ferrite from hard to soft magnetic material.

It can be concluded that different changes occur in the structural and magnetic properties of Mg substituted cobalt ferrite nanoparticles due to the rearrangements of divalent metal cations at different sites.

## References


[1] C. Sujatha, K. V. Reddy, K. S. Babu, A. R. Reddy, K. Rao, Ceramics International **38**, 5813 (2012).
[2] Y. Qi, Y. Yang, X. Zhao, X. Liu, P. Wu, F. Zhang, et al., Particuology **8**, 207 (2010).
[3] S. Prathapani, M. Vinitha, T. V. Jayaraman, D. Das, Journal of Applied Physics **115**, 17A502 (2014).
[4] B. V. Prasad, K. Ramesh, A. Srinivas, Journal of Superconductivity and Novel Magnetism **30**, 3523 (2017).
[5] H. Mund, B. Ahuja, Materials Research Bulletin **85**, 228 (2017).
[6] L. Kumar, M. Kar, Journal of Magnetism and Magnetic Materials **323**, 2042 (2011).
[7] X. Meng, H. Li, J. Chen, L. Mei, K. Wang, X. Li, Journal of Magnetism and Magnetic Materials **321**, 1155 (2009).
[8] Y. Cedeño-Mattei, O. Perales-Pérez, O. Uwakweh, Materials Chemistry and Physics **132**, 999 (2012).
[9] A. Giri, E. Kirkpatrick, P. Moongkhamklang, S. Majetich, V. Harris, Applied Physics Letters **80**, 2341 (2002).

[10] R. Panda, R. Muduli, G. Jayarao, D. Sanyal, D. Behera, Journal of Alloys and Compounds. **669**, 19 (2016).
[11] K. Khalaf, A. Al-Rawas, H. Widatallah, K. Al-Rashdi, A. Sellai, A. Gismelseed, et al., Journal of Alloys and Compounds **657**, 733 (2016).
[12] V. Vinayak, P. P. Khirade, S. D. Birajdar, P. Gaikwad, N. Shinde, K. Jadhav, Int. Adv. Res. J. Sci. Eng. Technol. **2**, 55 (2015).
[13] A. Pandit, A. Shitre, D. Shengule, K. Jadhav, Journal of Materials Science **40**, 423 (2005).
[14] A. Hassadee, T. Jutarosaga, W. Onreabroy, Procedia Engineering **32**, 597 (2012).
[15] I. Gul, W. Ahmed, A. Maqsood, Journal of Magnetism and Magnetic Materials **320**, 270 2008.
[16] B. P. Jacob, S. Thankachan, S. Xavier, E. Mohammed, Journal of Alloys and Compounds **578**, 314 (2013).
[17] X. Jiao, D. Chen, Y. Hu, Materials Research Bulletin **37**, 1583 (2002).
[18] A. Košak, D. Makovec, A. Žnidaršič, M. Drofenik, Journal of the European Ceramic Society, **24**, 959 (2004).
[19] A. Sutka, G. Mezinskis, Frontiers of Materials Science **6**, 128 (2012).
[20] M. Margabandhu, S. Sendhilnathan, S. Senthilkumar, D. Gajalakshmi, Brazilian Archives of Biology and Technology **59**, (2016).
[21] M. G. Naseri, E. B. Saion, H. A. Ahangar, A. H. Shaari, M. Hashim, Journal of Nanomaterials **2010**, 75 (2010).
[22] M. Sangmanee, S. Maensiri, Applied Physics A **97**, 167 (2009).
[23] S. Chakrabarty, M. Pal, A. Dutta, Materials Chemistry and Physics **153**, 221 (2015).
[24] Z. T. Khodair, A. A. Kamil, Y. K. Abdalaah, Physica B: Condensed Matter. **503**, 55 (2016).
[25] S. Muthurani, M. Balaji, S. Gautam, K. H. Chae, J.-H. Song, D. P. Padiyan, et al., Journal of Nanoscience and Nanotechnology **11**, 5850 (2011).
[26] M. George, S. S. Nair, K. Malini, P. Joy, M. Anantharaman, Journal of Physics D: Applied Physics **40**, 1593 (2007).
[27] A. R. Denton, N. W. Ashcroft, Physical Review A **43**, 3161 03/01/ 1991.
[28] T. Javed, A. Maqsood, A. A. Malik, Journal of Superconductivity and Novel Magnetism **24**, 2137 (2011).
[29] R. Sridhar, D. Ravinder, K. V. Kumar, Advances in Materials Physics and Chemistry **2**, 192 (2012).
[30] S. Gowreesan, A. R. Kumar, Journal of Materials Science: Materials in Electronics **28**, 4553 (2017).
[31] M. G. Naseri, E. B. Saion, H. A. Ahangar, A. H. Shaari, Materials Research Bulletin **48**, 1439 (2013).
[32] C. Ragupathi, J. J. Vijaya, L. J. Kennedy, M. Bououdina, Ceramics International **40**, 13067, (2014).
[33] D. S. Nikam, S. V. Jadhav, V. M. Khot, R. Bohara, C. K. Hong, S. S. Mali, et al., RSC Advances **5**, 2338 (2015).
[34] A. Franco Jr, F. e Silva, V. S. Zapf, Journal of Applied Physics **111**, 07B530 (2012).
[35] A. Manikandan, J. J. Vijaya, M. Sundararajan, C. Meganathan, L. J. Kennedy, M. Bououdina, Superlattices and Microstructures **64**, 118 (2013).
[36] I. Nlebedim, N. Ranvah, Y. Melikhov, P. Williams, J. Snyder, A. Moses, et al., IEEE Transactions on Magnetics **45**, 4120 (2009).
[37] Y. Köseoğlu, F. Alan, M. Tan, R. Yilgin, M. Öztürk, Ceramics International **38**, 3625 (2012).
[38] P. Aghav, V. N. Dhage, M. L. Mane, D. Shengule, R. Dorik, K. Jadhav, Physica B: Condensed Matter **406**, 4350 (2011).
[39] A. Druc, A. Dumitrescu, A. Borhan, V. Nica, A. Iordan, M. Palamaru, Open Chemistry **11**, 1330 (2013).
[40] R. S. Yadav, I. Kuřitka, J. Vilcakova, J. Havlica, J. Masilko, L. Kalina, Advances in Natural Sciences: Nanoscience and Nanotechnology **8**, 45002 (2017).